Source: Solid Freeform Fabrication 2021: Proceedings of the 32nd Annual International Solid Freeform Fabrication Symposium – An Additive Manufacturing Conference

Title: Microstructure and Mechanical Test Data Alignment for Additive Manufacturing Data Registration

Authors:

Shaw C. Feng, Albert T. Jones, and Yan Lu, Engineering Laboratory, National Institute of Standards and Technology, Gaithersburg, MD 20899

Abstract

Melt pool monitoring, microstructure, and mechanical property data are becoming increasingly available and important in additive manufacturing (AM). These data along with data analytics tools can be used to ensure the part's quality and accelerate the qualification process. A major impediment to correlating these types of data is that they are obtained in different local coordinate systems. To establish the required process-microstructure-property relationships, these data must also be aligned with other build data such as build commands. This paper proposes an innovative data registration procedure to correlate and organize these different types of data.

1. Introduction

In recent Additive Manufacturing (AM) research efforts, the focus has been on 1) understanding the material-process-structure-property relationships [NASA 2021] [DoD2016], 2) aligning multi-modal data into a common reference coordinate system [Feng2020-1] [Lu2020], 3) providing the metadata on the needed context information about sensors for identifying relationships among the different sensor data [Feng2020-2], and 4) using those relationships to improve process control and part quality [Mani 2017-1]. Successfully executing these tasks relies on a variety of microstructure measurement methods including scanning electron microscopy (SEM), Electron Backscattering Diffraction (EBSD) SEM, Energy Dispersive Scattering (EDS), and X-ray Diffraction Spectroscopy (XDS). These methods and their various data outputs can be used to study both microstructure and residual stress of parts of AM parts.

A systematic organization of the microstructure measurement data is needed for downstream applications, such as data analysis, process control, and part qualification. For example, controlling AM processes for an equiaxed grain structure can improve component quality [Todaro2020]. Utilizing microstructure data in addition to mechanical test data has the potential to accelerate both material and part qualification processes, while reducing the need for AM builds and test specimens [Seifi2016]. A critical aspect of microstructure and mechanical test data organization involves registering the data. The benefits of registering data are associated with the **FAIR** principles for scientific data management and stewardship [Wilkinson 2016]. **F** is for finding data based on unique identifiers. **A** is for accessing that data with defined protocols that include the known times, locations, and approvals. **I** is for interoperability by using shared terminology in machine-interpretable format. **R** is for reusing existing data in future applications.

For AM, the benefits of using these principles are improved data alignment, data fusion, and defect tracing.

In this paper, the "data" was collected from AM processes, several different types of microstructure characterization, and tensile tests. Collectively, this data provides critical inputs to process-structure-property relationship analysis of parts fabricated using a Laser-based Powder Bed Fusion of Metals (PBF-LB/M) [iso/astm 52911]. To perform this analysis, however, it is important to align the melt pool monitoring data with a cross-section microstructural data of AM parts and with mechanical test measurements. Specifically, the data alignment of melt pool data and fracture surface with microstructure on the fracture was not available. The resulting alignment can be used to better understand the relationships between microstructural morphology and composition and mechanical properties. The resulted structure-property relationship can be used to control the process and qualify the fabricated parts.

Section 2 reviews currently available research results that correlate process data, microstructural data, and property data. The imbedded techniques for data alignment are also reviewed. Potential gaps are then identified. Section 3 describes the common coordinate system used for AM data alignment and registration. Section 4 proposes a data alignment method for microstructural data. Section 5 proposes a data alignment method for tensile test data. Section 6 discusses the methods from the application point of view. Section 7 concludes the methods with possible future work.

2. Status of Microstructure and Tensile Test Data

This section reviews available research activities that need to relate microstructure images with process parameters and mechanical properties for exploring the relationships among process, structure, and property in laser-based additive manufacturing for metals. Potential gaps are then identified for developing a formal methodology to related data from different sensors.

2.1 Review of Research on Microstructure and Tensile Test Data Correlations

As noted above, there is a critical need to align and correlate microstructure data with in-process data to analyze the causes and the consequences of part quality problems [Galy2018]. Sames et al. [Sames2016] provided examples of this need to correlate microstructural features including defects, pores, and cracks to the scanning strategies in the AM process. Franscois et al. [Franscois2017] modeled the grain growth direction and melt pool heating and cooling to show that grain orientation and size are related to the melt pool moving direction. King et al. [King2015] also proposed simulation models to show the relationships among process, material, and property. The authors argued that estimating experimental correlations using measurements of physical phenomena is difficult. More correlations among melt pool, microstructure, residual stress, and mechanical property are discussed as follows.

2.1.1 Melt Pool and Microstructure Data Alignment

Many research results about melt pool, solidification, and microstructural evolutions have become available. Lee et al [Lee2016] described the significant effects of melt pool flow on the temperature gradient and solidification rate, which impact the grain growth, size, and orientation.

The paper shows that the melt pool travel direction and heat gradient determine the formation of columnar and cellular grains. Chadwick et al. [Chadwick2021] showed a Rosenthal-based simulation of nucleation and grain growth in the temperature gradient driven by the moving laser beam. Zhang et al. [Zhang2019] used a different melt pool modeling technique to study melt-pool temperature distribution and the cooling rate at the melt pool boundaries and their effects on microstructural evolution. Grain growth, grain sizes, grain shapes, and grain orientations were simulated and showed the relative positions and orientations of grain structures to melt pool and its moving direction. A report from Argonne National Laboratory [Argonne20/40] describes relationships between the Metal Additive Manufacturing (MAM) process and the microstructure of the material. Modeling and simulation for prediction of initial microstructures to describe geometrical relationships of melt pool and microstructural evolution are also reported in [Argonne20/21].

There are studies on the correlations among process, microstructure, and property for laser-based additive manufacturing for metals, e.g., Gu et al. [Gu2012]. This study includes powder melting, microstructural evolution, grain structures, and mechanical properties. Specifically, Gu et al. [Gu2018] studied microstructures within the melt pool in the LPBF process. In the study, grain growth direction, grain size, and grain shape are shown relative to the scan direction and build direction in the powder bed. Cellular dendrite, columnar dendrite, equiaxed grain are predicted in the cross-section and the longitudinal cross-section of the melt pool. Sahoo et al. [Sahoo2016] proposed a model to simulate the thermal profile of a melt pool in the scan direction. There were two purposes. The first was to correlate the phase profile of the metal at different solidification times. The second was to predict grain growth including the growth rate and microstructure evolution in the solidification process. Zinoviev et al. [Zinoviev2016] used a Goldak double ellipsoid in a local coordinate system to define the melt-pool shape including its dimensions and moving direction. The authors simulate and measure the grain structures originated from the polycrystalline substrate. The substrate, melt pool, and crystal orientation needed to be correlated, but some details on the correlations were unavailable. Knapp et al. [Knapp2019] simulated melt-pool geometry and graphically overlaid it on optical images of columnar grains. This overlapping allows the researchers to compare grain-growth direction to the solidification of flowing metal liquid in the melt pool. This comparison is made in both cross-section in the moving direction and cross-section perpendicular to the moving direction.

Shi et al. [Shi2020] related the microstructural evolution to both the melt-pool shape and the laser-beam shape. The purpose is to control grain growth, size, and orientation and thereby optimize mechanical properties. The melt pool temperature, size, shape, and moving speed are closely relate to microstructures in traverse, longitudinal, and horizontal directions relative to the melt-pool shape and laser-moving direction. Kelly et al. [Kelly2004] studied the macrostructure and microstructure in a laser-deposited part relative to process parameters including layer thickness and laser-beam dimensions. The microstructures were observed using an optical microscope. However, in the study, the image coordinate system and the microscope coordinate system were not explicitly correlated.

Gu et al. [Gu2013] studied the effects of the energy density of the laser beam and scanning speed on the microstructure and the porosity on melting stainless-steel powders. The build direction, laser scanning path, and energy-density readings were defined on the build plate coordinate system. The microstructure images, however, are on the coordinate system local to the scanning electron microscope (SEM). The observed pores, unmelted powders, and contaminates on the SEM images are qualitatively related to the energy density readings in the build-plate coordinate system.

2.1.2 Scanning Strategy and Microstructure Data Alignment

Stoudt et al. [Stoudt2020] used the build-plate coordinate system to align microstructural-data coordinate system and process-data coordinate system. The authors oriented different images from SEM, Electron Backscattering Diffraction (EBSD) microscopy, Energy Dispersive Spectroscopy (EDS) to study the grain size, grain orientation, inclusions, and grain shape in different portions of the test part. This is needed because of different temperature gradients and cooling rates. Zitelli et al. [Zitelli2019] reviewed the microstructures and process-related defects in LPBF for fabricating stainless steel. The authors studied samples that were built in different orientations in the build plate coordinate system. Optical micrographs showed the microstructure of the samples in the build direction. Different grain sizes, orientations, and shapes are observed using EBSD. These microstructures are compared with respect to different laser scanning strategies. Different samples are then put under a tensile test, which showed different mechanical properties. Pham et al. [Pham2020] investigated the role of side branching during grain growth in the solidification process. The direction and length in side-branching play an important role that determines the grain shape and size. The authors tried to align side-branching directions with respect to the build direction and melt-pool moving direction. The investigation showed that different, layer-by-layer, scanning strategies can greatly influence the side branching and, thus, alter the microstructure in the fabricated part.

Koepf et al. [Koepf2018] introduced a method to correlate microstructural images with scanning strategies. Grain growth directions on individual layers were correlated using a melting and remelting simulation, which was created to study the effects of scanning strategy to microstructures. Arisoy et al. [Arisoy2017] also related scan strategy, process parameters, to microstructure with correlations of melt pool, grain structure, and process parameters. Chen et al. [Chen2012] compared a phase-field modeling method with direct, real-time observations using synchrotron X-ray radiography. In their study, the authors used a graph-based technique to correlate grain growth direction, shape, and size with the melt-pool shape, cooling direction, and thermal gradients. Watring et al. [Watring2020] reported the effects of build orientation coupled with laser-energy density on the microstructure and mechanical properties of Inconel 718 parts created using an LPBF process. The build directions of different coupons were correlated with the lack-of-fusion defects in the coupons, the crystal structures, and the mechanical properties. Hanzl et al. [Hanzl2014] investigated the influence of process parameters on the mechanical properties of AM built by the LPBF process. The authors described part orientations relative to the build plate, melting directions, scanning direction, and layer thickness to the mechanical properties including tensile strengths and elongations. Benzing et al. [Benzing2020] tracked defects and

microstructural heterogeneities in tensile coupons. The authors (1) correlated the coupon orientation relative to the build plate coordinate system, (2) located the defects observed in images of the fracture surface, and (3) correlated fracture, microstructure, to the scanning and melting during processing.

2.1.3 Melt Pool and Fracture Data Alignment

Qiu et al. [Qiu2015] related the role of melt pool in influencing the porosity development in the LPBF process. The authors identified pores in SEM images on a local Coordinate System (CS). The melt-pool size, shape, and moving direction are in another local CS. The author correlates the two using a thermal, fluid-flow simulation with melt-pool images taken with a high-speed camera. The images are in, yet, another local CS based on the camera CS. Vastola et al. [Vastola2018] developed a model to predict porosity in LPBF in the keyholing region. The authors tried to relate porosity in the model with the melt-pool model that predicts keyholing effects. All the coordinates are in the simulation CS. Zheng et al. [Zheng2019] proposed a method for porosity formation based on the moving melt pool during the scan in LPBF. In the paper, the authors showed the correlation between the SEM image of microstructure and the simulated melt-pool geometry. The purpose was to study the formation of different microstructures based on different energy densities according to laser power and scan speed.

Kruth et al. [Kruth2010] conducted experiments to better understand the influence of scanning strategies on microstructure and impacts of the microstructure on mechanical properties of the coupons in LPBF/LB-M. The resulting correlations of melt-pool shape and size, grain sizes and orientations, and mechanical property tests were estimated. The need of using a common reference CS was obvious and could have helped in aligning the datasets. Bartlett et al. [Bartlett2018] correlated the residual stress from measurements with process variables including layer thickness, stiffness of the part, and stiffness of the base. The scanning paths were correlated with the developed in-plane residual stress of a scanned layer. Bauereiss et al. [Bauereiss2014] observed defect development, formation, and propagation during a PBF/LB-M process. The melt pool was observed in the build-plate CS; but defect formation and propagation were observed in microscope CS. The pores and crack development and the melt pool moving direction are in two separate CSs. They were graphically overlaid. Lewandowski et al. [Lewandowski2016] reviewed tensile and hardness tests on many coupons that were built in different orientations. The paper emphasized the importance of microstructures, fractures, and properties correlations on the geometric alignment.

2.2 Gaps in Process, Microstructure, and Property Data Correlations

From the literature review above, we find the process data, microstructure data, and mechanical property data are primarily overlaid graphically using the build plate CS. Studies that focus on nominal process parameters, average microstructure properties, and mechanical tests can simply use the build plate CS as the center of aligning related data. Correlating melt pool or individual laser track data, e.g., melt pool monitoring data, to microstructure and fracture surfaces is more complicated. A formal method to align melt pool, scanned track, coupon, sample, specimen, and fracture are not well correlated geometrically. Consequently, tracing defects found in the

samples to process parameters, such as laser power, scan speed, scan pattern, and layer thickness is difficult. Specifically, there are following barriers in data correlations. The authors identified the following three barriers to data correlations.

(1) Melt pool geometry and other local CSs are not well correlated to the build platform CS.

(2) The test-coupon CS is not correlated with the build platform CS even though standards exist for this, e.g., ISO/ASTM 52921 [iso52921].

(3) Few methods exist to locate the fracture surface relative to the coupon CS.

A proposed data alignment procedure to remove these barriers is described in the following three sections.

3. Build Plate Coordinate System and Melt Pool Data Alignment

A melt pool is generated after the laser beam melts the powders. As shown in Figure 1, the central pixel of the laser spot in the image is used as the reference point in the alignment. The laser spot center in the coaxial-camera CS can be estimated using the intensity gradient of the melt pool shown in the image. The laser spot center on the scan path is in the scanning laser CS.

The relative orientation between the image ("from") and the layer ("To") can be computed using an appropriate image calibration method. An image calibration artifact with black-and-white grids may be used to measure the relative orientation difference between the orientation in the coaxial-camera coordinate system and the orientation in the laser scanning coordinate system. To align the artifact to the build platform, one edge of the black-and-white-grid artifact must be aligned with one edge of the build platform. More detailed information can be found in [Feng2020-1].

The build platform CS can be used as the primary reference coordinate system in the layer-by-layer scanning process. Figure 1 shows the coordinate system on the build platform [iso 52921]. A staring camera is used to take an image of the build platform, as shown in Figure 2. The image is the X-Y plane, and the Z direction is perpendicular to the X-Y plane. The Z-X plane can be established by the mid-plane of the front plane and rear plane. How to detect edges is described below on edge-fitting. For fitting the two edges, both lines must be parallel. The Y-Z

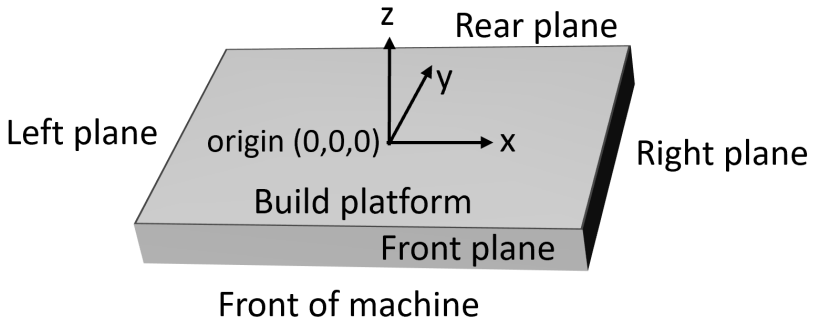

Figure 1 Build platform coordinate system

plane can be established by the mid-plane of both the left plane and right plane and must be perpendicular to both X-Y and Z-X planes. The intersection of the three planes is the origin.

If a rectangular part occupies a small region on the build platform, as shown in the upper right corner of Figure 2, the field of view of the staring camera is only a subarea of the build platform. Note that the image of the part is distorted due to the spherical lens and its thickness. To establish a local CS (X_{local}, Y_{local}) is thus needed. The same method as above can be applied. Note that X_L and X_{local} are parallel to each other, and Y_L and Y_{local} are parallel to each other since the two CSs are created by the same laser beam. The build platform CS is established from the build-plate shape. The laser CS is established from the build platform CS. Finally, a local CS is established from the laser beam CS.

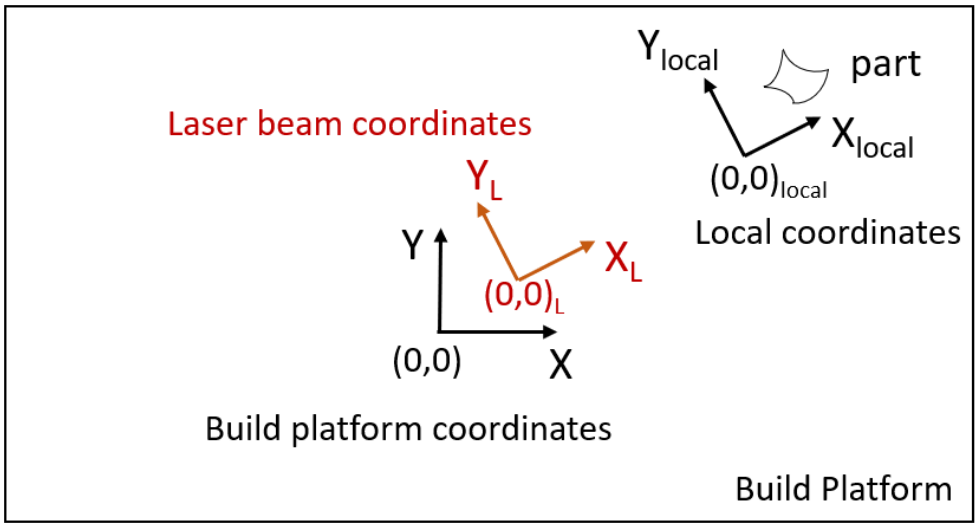

Figure 2 Staring camera and build platform coordinate systems

4. Microstructural Data Alignment

This section describes a method for establishing a specimen Coordinate System (CS) relative to the Build Plate CS. The section also describes possible microstructural data sources. Then, a method to establish related CSs is introduced.

Possible microstructural data sources include microscopes and spectroscopes. Optical microscopy (OM) is commonly used in microstructural analysis. OM images can provide information on the melt pool depth in both longitudinal and traverse directions, melt pool/track cross-section, grain morphology, and distribution of porosity. Scanning electron microscopy (SEM) is frequently used to predict some or all primary phases, grain size, aspect ratio, dendritic vs. equiaxed microstructure, and elemental segregation within the thick and thin features of an AM part. These microstructures are determined by the temperature gradient and cooling rate, which are determined by melt pool characteristics. SEM images can be observed from different view angles, such as transverse or longitudinal views of the part. Electron backscatter diffraction (EBSD) SEM can provide detailed information on grain size, grain orientation, inclusions, and defects in grain boundaries. Energy dispersive spectroscopy (EDS) provides elemental analysis of the material in microstructural analysis. Powder X-Ray Diffraction (PXRD) is used to identify the phases and

phase fractions within the specimens, including the most common precipitates. PXRD allows us to evaluate phase composition, crystallite size, strain and defect defects. PXRD also allows time-resolved studies [Cheng2017]. Powder X-ray diffraction measurements and subsequent analysis can be used to identify the phases and phase fractions within the specimens, including the most common precipitates. Ultra-small-angle X-ray scattering (USAXS) instrument uses ultra-small-angle X-ray scattering to obtain information about a sample's microstructure over a larger size range from micrometers to below one nanometer. The pinhole small-angle X-ray scattering (SAXS) technique is used to study the small length scales in the nanometer range. The wide-angle scattering (X-ray diffraction) technique is used to obtain the phase information, including the most common precipitates. This work focuses only on OM, SEM, and EBSD SEM.

This work focuses on optical and electron microscopy including electron backscatter diffraction (EBSD). Grain structures can be observed by two means. First, a sample is cut from the part fabricated for microstructural analysis. No mechanical testing is involved. Second, an observation is made after a mechanical test (e.g., tensile or fatigue). The microstructure can be observed using a microscope to take images of microstructural features in the fracture, such as pores, cracks, unmelted powders, and soots. Using SEM, grain structure including size, orientation, and phase can be analyzed from SEM images. A coupon is used for destructive evaluation. It is fabricated in the Laser CS (X_L, Y_L, Z_L). See Figure 3. A sample is cut from the coupon and has its own CS based on the design. The local coupon CS is (X_C, Y_C, Z_C). It is used to reference the specimen. After the cut, local sample CS is (X_S, Y_S, Z_S). Images can be taken using a microscope. Since microstructures are very small comparing to the average melt pool size, the center of the viewing area can represent the location of the microstructure. The orientation is in the direction of Z_S. The transformation between CS (X_S, Y_S, Z_S) and CS (X_C, Y_C, Z_C), as well as that between CS (X_C, Y_C, Z_C) and CS (X_L, Y_L, Z_L) has to be obtained first. Then, the location and orientation of the microstructure can be transformed to the Laser CS for relating to melt pools and layers in the build. Hence, issues found from analyzing the images including melting, melt pool formation, cooling, and solidification can then be traced back to the in-process monitoring.

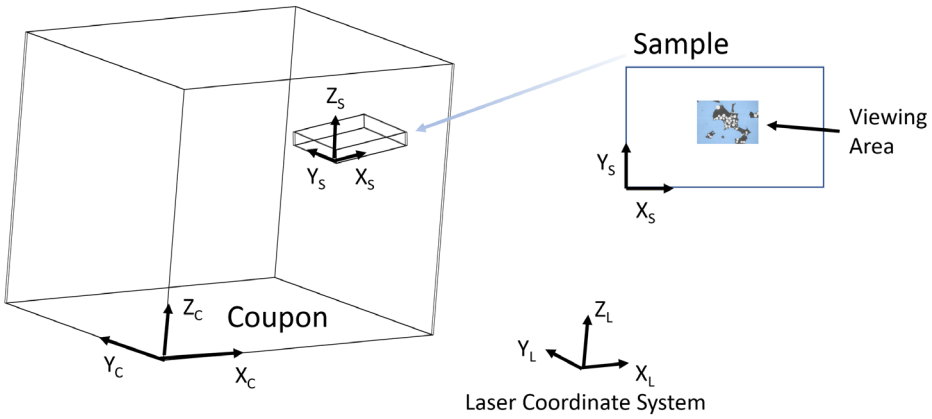

Figure 3 Microstructural Sample Coordinate System

5. Test Coupon Fracture Coordinate System and Build Plate Coordinate System

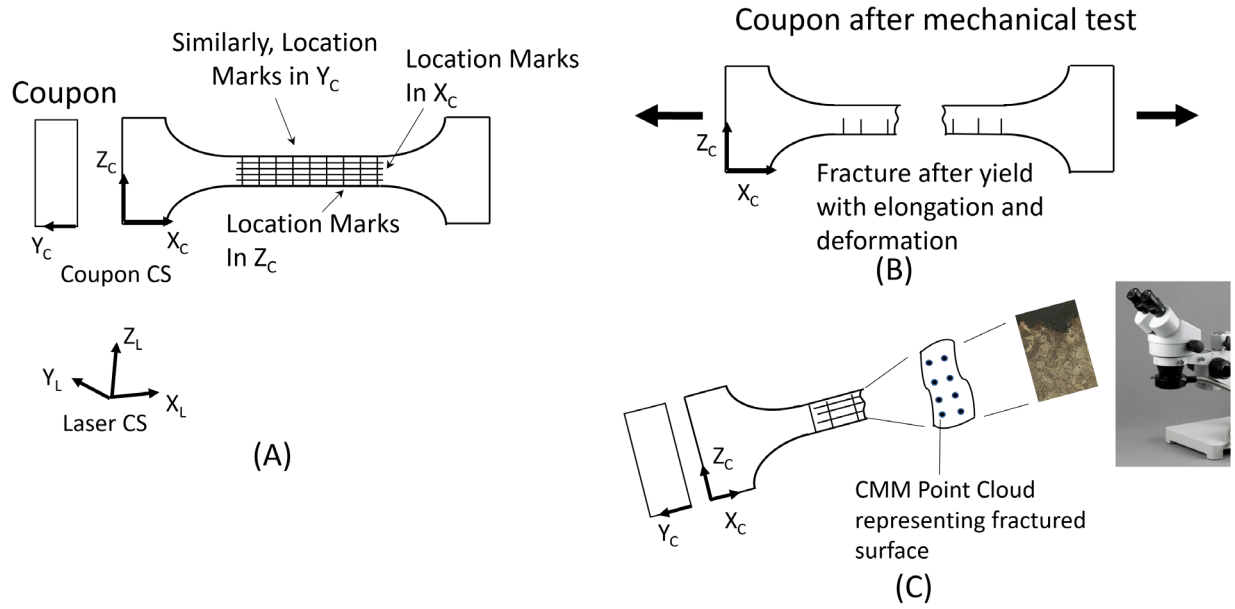

Figure 4 Property test data coordinate systems

This section describes a method for relating both the coupon CS to the build plate CS and the fractured surface CS to the coupon CS. For imaging a fracture cross-section, a microscope is used (see Figure 4). The microstructures include pores, ruptures, soots, unmelted powders, and striations. Typically, coupons that are used as tensile-test specimens are fabricated at the same time with the part in the same build. The properties of a coupon are like those of the part. During mechanical testing, specimens are deformed with elongation, fracture, and distortion. To trace the defects to the process, we need to relate fracture surface and point features on the surface to the original shape. Figure 4 (A) shows a specimen directly fabricated from an AM process, where the specimen is also a coupon, in the CS (X_C, Y_C, Z_C), as shown in Figure 4 (A). Because of the deformation, location marks are placed on the coupon. Location marks in the X_C direction indicate the original X in the coupon CS. Similarly, location marks in the Y_C direction indicate the original Y location in the coupon CS. Lastly, location marks in the Z_C direction indicate the original Z location in the coupon CS.

After the coupon is fractured, the fractured portions are elongated because the applied force exceeds the yield strength. The marks preserve the original positions. The fracture surface can then be related to the coupon CS in the X_C direction, as shown in Figure 4 (B). The features on the fractured surface can also be related to the X and Y coordinates (X_C, Y_C) in the coupon CS, as shown in Figure 4 (C).

6. Discussion

In this paper, we present methods to align data generated from AM in-process monitoring, ex-situ microstructure inspections, and mechanical tests based on a common coordinate system defined in ISO/ASTM 52921 – the built-platform coordinate system. The laser marks, which are used to reference the origin and orientation of the laser-beam coordinate systems on the build

platform, can create uncertainty due to the variations in the laser power intensity and the galvanometer positioning. These variations can affect the laser-mark image quality.

For microstructure data alignment, a microscopic image is first aligned with the sample CS, which is in the build plate CS. We used only SEM images since they can be located and oriented relative to the local CS of the specimen. Other images from XRD, EPS, and ultrasmall-, small-, and wide-angle X-ray scattering are more complicated and in the very small scale, i.e., micrometer to nanometer scale. They can be dealt with later when needs are present. SEM specimens for microstructural data analysis are cut and polished. Because of the precision of the cut, the location and orientation of the specimen relative to the sample CS can be easily measured and reported from the instrument that is used to prepare the sample and specimen.

Further, we propose a method to align the mechanical-test coupon CS with the build plate CS. Location marks in Figure 6 are usually made manually. Manual operations can introduce uncertainty in the marks of the coupon. Tools including fixtures can be designed and manufactured to better mark the original positions of the test coupon with higher precision.

Overall, the various methods introduced in this paper can align data collected from different sensors, microscopic instruments, and tested coupons. With data alignment, features in microstructural data, such as voids, unmelted particles, cracks, inclusions, grain orientation, and grain size can be traced to process parameters including melt pool size for root cause analysis. Challenges remain in meeting industry needs to use various cases in different materials, process parameters, and design models [Mani2017-2].

7. Conclusions and Future work

This paper proposes a procedure for correlating microstructural data with both process data and property data. Microstructural images, which are collected using an EBSD SEM instrument, are necessary to predict mechanical properties in the part. A method to correlate microstructural data with property data has been described. Microstructure images are in the specimen local CS, which is in the sample CS. We also propose a method to relate mechanical property data in the coupon CS to the build plate CS.

The paper also describes a method to correlate microstructural data with AM process data. Process parameter data, including laser power, beam size, and scanning speed influence microstructure including grain size, grain orientation, and phases are in the build plat CS. The proposed method is to align process data in the built-platform CS to microstructural data in the specimen CS. The test specimens are part of the sample and is placed in the local sample CS. The Sample is in the laser CS. The Laser CS is related to the build plate CS using two mutually perpendicular, thin-laser marks. To this end, process data, microstructural data, and mechanical property data are all in a common build-platform CS. Grain locations and orientations are thus aligned with process data and property data.

Further research activities are suggested as follows. First, any correlation of the laser CS to the build plate CS should be further investigated using a smaller laser beam to make finer and more precise marks to locate the laser CS on the build plate. Second, we propose setting fiduciary

marks in SEM images for the purpose of aligning microstructural data in the sample to microstructural data in the sample CS. Lastly, it is a good idea to try to improve the method to determine the fracture surface's location and orientation in the coupon so that features shown in the fracture can be better located in the coupon CS.

Disclaimer

Certain commercial equipment, instruments, or materials identified in this paper are not intended to imply recommendation or endorsement by the National Institute of Standards and Technology, nor is it intended to imply that the materials or equipment identified are necessarily the best available for the purpose. Any opinions, findings, conclusions, or recommendations expressed in this material are those of the authors and do not necessarily reflect the views of NIST or any other supporting U.S. government or corporate organizations. Further, this material is declared a work of the U.S. Government and is not subject to copyright protection in the United States of America.

References

[1] [NASA2021] NASA / NIST / FAA Technical Interchange Meeting on Computational Materials Approaches for Qualification by Analysis for Aerospace Applications, NASA/TM–20210015175, May 2021.

[2] [DoD2016] Department of Defense Additive Manufacturing Roadmap, Final Report, #88ABW-2016-5841, November 2016.

[3] [Feng2020-1] Feng, S., Lu, Y., and Jones, A. (2020) "Measured data alignments for monitoring metal additive manufacturing processes using laser powder bed fusion methods," Proceedings of ASME 2020 International Design Engineering Technical Conferences and Computers and Information in Engineering Conference, IDETC/CIE 2020-22478.

[4] [Lu2020] Lu, Y., Yang, Z., Kim, J., Cho, H., and Ho, Y., "Camera-based Coaxial Melt Pool Monitoring Data Registration For Laser Powder Bed Fusion Additive Manufacturing," Proceedings of the ASME 2020 International Mechanical Engineering Congress and Expo, November 2020, paper #: IMECE2020- 23180.

[5] [Feng2020-2] Feng, S., Lu, Y., and Jones, A. (2020) "Meta-data for in-situ monitoring of laser powder bed fusion processes," Proceedings of ASME 2020 Manufacturing Science and Engineering Conference, MSEC 2020-8344.

[6] [Mani 2017-1] Mani, M., Lane, B., Donmez, A., Feng, S., and Moylan, S., "A Review on Measurement Science Needs for Real-time Control of Additive Manufacturing Metal Powder Bed Fusion Processes," International Journal of Production Research, Volume 55, Issue 5, 2017, pp. 1400-1418.

[7] [Todaro2020] Todaro, C., Easton, M., Qiu, D., et al., "Grain structure control during metal 3D printing by high-intensity ultrasound," Nature Communications, 2020, https://www.nature.com/articles/s41467-019-13874-z

[8] [Seifi2016] Seifi, M., Salem, A., Beuth, J., Harrysson, O., and Lewandowski J., "Overview of materials qualification needs for additive manufacturing," Journal of Materials, Vol. 68, No. 3, 2016, pp. 747 – 764.

[9] [Wilkinson 2016] Wilkinson, M. et al., "The FAIR Guiding Principles for scientific data management and stewardship," Scientific Data, 2016, DOI: 10.1038/sdata.2016.18.
[10] [ISO/ASTM 52911] ISO/ASTM 52911-1:2019, Additive manufacturing - Design - Part 1: Laser-based powder bed fusion of metals, International Organisation for Standardization, 2019.
[11] [Galy2018] Galy, C., Guen, E., Lacoste, E., and Arvieu, C., "Main defects observed in aluminum alloy parts produced by SLM: from causes to consequences," J. Additive Manufacturing, Vol. 22, 2018, pp. 165 – 175.
[12] [Sames2016] Sames, W., List, F., Pannala, S., Dehoff, R., and Babu, S., "The metallurgy and processing science of metal additive manufacturing," International Materials Reviews, Vol. 61, No. 5, 2016, pp. 315 – 360.
[13] [Francois2017] Francois, M., Sun, A., King, W., et al., "Modeling of additive manufacturing processes for metals: challenges and opportunities," Current Opinion in Solid State and Materials Science, Vol. 21, 2017, pp. 198 – 206.
[14] [King2015] King, W., Anderson, A., Ferenccz, R., Hodge, N., Kamath, C., Khairallah, S., and Rubenchik, A., "Laser powder bed fusion additive manufacturing of metals; physics, computational, and material challenges," Applied Physics Reviews, Vol. 2, 2015, #041204.
[15] [Lee2016] Lee, Y and Zhang, W., "Modeling of heat transfer, fluid flow and solidification microstructure of nickel-based superalloy fabricated by laser powder bed fusion," J. Additive Manufacturing, Vol. 12, 2016, pp. 178 – 188.
[16] [Chadwick2021] Chadwick, A. and Voorhees, P., "The development of grain structure during additive manufacturing," Acta Materialia, Vol. 211, 2021, #116862.
[17] [Zhang2019] Zhang, Z, Tan, X., Hu, C., Ge, P., Wan, Z., Li, J., and Wu, Q., "Numerical methods for microstructural evolutions in laser additive manufacturing," J. Computers and Mathematics with Applications, Vol. 78, 2019, pp. 2296 – 2307.
[18] [Argonne2020-1] Applied Materials Division, "Survey of methods for predicting material performance from material microstructure for advanced manufacturing technologies," Argonne National Laboratory, ANL-20/40, 2020.
[19] [Argonne2020-2] Applied Materials Division, "Survey of modeling and simulation techniques for predicting initial microstructures for advanced manufacturing technologies," Argonne National Laboratory, ANL-20/21, 2020.
[20] [Gu2012] Gu, D., Meiners, W., Wissenbach, K., and Poprawe, R., "Laser additive manufacturing of metallic components: material, processes and mechanisms," International Materials Reviews, Vol. 57, No. 3, 2012, pp. 133 – 164.
[21] [Gu2018] Gu, D., Shi, Q., Lin, K., and Xi, L., "Microstructure and performance and underlying thermal mechanisms of Ni-based parts fabricated by selective laser melting," J. Additive Manufacturing, Vol. 22, 2018, pp. 265 – 278.
[22] [Sahoo2016] Sahoo, S. and Chou, K., "Phase-field simulation of microstructure evolution of Ti-6Al-4V in electron beam additive manufacturing process," J. Additive Manufacturing, Vol. 9, 2016, pp. 14 – 24.
[23] [Zinoviev2016] Zinoviev, A., Zinovieva, O., Ploshikhin, V., Romanova, V., and Balokhonov, R., "Evolution of grain structure during laser additive manufacturing simulation by a cellular automata method," J. Materials and Design, Vol. 106, 2016, pp. 321 – 329.

[24] [Knapp2019] Knapp, G., Raghavan, N., Plotkowski, A., and DevRoy, T., "Experiments and simulations on solidification microstructure for Inconel 718 in powder bed fusion electron beam additive manufacturing," J. Additive Manufacturing, Vol. 25, 2019, pp. 511 – 521.
[25] [Shi2020] Shi, R., Khairallah, S., Roehling, T., Heo, T., McKeown, J., and Matthews, M., "Microstructural control in metal laser powder bed fusion additive manufacturing using laser beam shaping stragegy," Acta Materialia, Vol. 184, 2020, pp. 284 – 305.
[26] [Kelly2004] Kelly, S. and Kampe, S., "Microstructural evolution in laser-deposited multilayer Ti-6Al-4V builds: Part I. Microstructural characterization," Metallurgy and Materials Transaction A, Vol. 35A, 2004, pp. 1861 - 1867.
[27] [Gu] Gu, H., Gong, H., Pal, D., Rafi, K., Starr, T., and Stucker, B., "Influences of energy density on porosity and microstructure of selective laser melted 17-4PH stainless steel," Proceedings of Solid Freeform Fabrication Symposium, 2013, pp. 474 – 489.
[28] [Stoudt2020] Stoudt, M., Williams, M., Levine, L., Creuziger, A., Young, S., Heigel, J., Lane, B., and Phan, T., "Location-specific microstructure characterization within IN625 additive manufacturing benchmark test artifacts," J. Integrating Materials and Manufacturing Innovation, Vol. 9, 2020, pp. 54 – 69.
[29] [Zitelli2019] Zitelli, C., Folgarait, P., and Di Schino, A., "Laser powder bed fusion of stainless steel grades: a review," J. Metals, Vol. 9, 2019, #731.
[30] [Pham2020] Pham, M., Dovgyy, B., Hooper, P., Gourlay, C., and Piglione, A., "The role of side-branching in microstructure development in laser powder-bed fusion," Nature Communications, Vol, 11, 2020, #749.
[31] [Koepf2018] Koepf, J., Gotterbarm, M., Markl, M., and Koener, C., "3D multi-layer grain structure simulation of powder bed fusion additive manufacturing," Acta Materialia, Vol. 152, 2018, pp. 119 – 126.
[32] [Arisoy2017] Arisoy, Y., Criales, L., Oezel, T., Lane, B., Moylan, S., and Donmez, A., "Influence of scan strategy and process parameters on microstructure and its optimization in additively manufactured nickel ally 625 via laser powder bed fusion," Int. J. Adv Manufacturing Technologies, Vol. 90, 2017, pp. 1393 – 1417.
[33] [Chen2012] Chen, Y., Bongo, A., Xiao, N., Billia, B., Kang, X., Nguyen-Thi, H., Luo, X., and Li, D., "Quantitatively comparing phase-field modeling with direct real time observation by synchrotron X-ray radiography of the initial transient during directional solidification of an Al-Cu alloy," Acta Materialia, Vol., 60, 2012, pp. 199 – 207.
[34] [Watring2020] Watring, D., Benzing, J., Hrabe, N., and Spear, A., "Effects of laser-energy density and build orientation on the structure-property relationships in as-built Inconel 718 manufactured by laser powder bed fusion," J. Additive Manufacturing, Vol. 36, 2020, pp. 101425.
[35] [Hanzl2014] Hanzl, P., Zetek, M., Baksa, T., and Kroupa, T., "The influence of processing parameters on the mechanical properties of SLM parts," Procedia Engineering, Vol. 100, 2015, pp. 1405 – 113.
[36] [Benzing2020] Benzing, J., Liew, L., Hrabe, N., and DelRio, F., "Tracking defects and microstructural heterogeneities in meso-scale tensile specimens excised from additively manufactured parts," J. Experimental Mechanics, Vol. 60, 2020, pp. 165 – 170.

[37] [Qiu2015] Qiu, C., Panwisawas, C., Ward, M., Basoalto, H., Brooks, M., and Attallah, M., "On the role of melt flow into the surface structure and porosity development during selective laser melting," Acta Materialia, Vol. 95, 2015, pp. 72 –79.
[38] [Vastola2018] Vastola, G., Pei, Q., and Zhang, Y., "Predictive model for porosity in powder-bed fusion additive manufacturing at high beam energy regime," J. Additive Manufacturing, Vol. 22, 2018, pp. 817 – 822.
[39] [Zheng2019] Zheng, M., Wei, M., Chen, J., Zhong, C., Lin, X., and Huang, W., "A novel method for the molten pool and porosity formation modelling in selective laser melting," Intl. J. Heat and Mass Transfer, Vol. 140, 2019, pp. 1091 – 1105.
[40] [Kruth2010] Kruth, J., Badrossamay, M., Yasa, E., Deckers, J., Thijs, L, and Van Humeeck, J., "Part and material properties in selective laser melting of metals," the 16th Intl. Symp., on Electromachining, 2010, pp. 3 -14.
[41] [Bartlett2018] Bartlett, J., Croom, B., Burdick, J., Henkel, D., and Li, X., "Revealing mechanisms of residual stress development in additive manufacturing via digital image correlation," J. Additive Manufacturing, Vol. 22, 2018, pp. 1 – 12.
[42] [Bauereiss2014] Bauereiss, A., Scharowsky, T., and Koerner, C., "Defect generation and propagation mechanism during additive manufacturing by selective beam melting," J. of Material Processing Technology, Vol. 214, 2014, pp. 2522 – 2528.
[43] [Lewandowski2016] Lewandowski, J. and Seifi, M., "Metal additive manufacturing: A review of Mechanical Properties," Annu. Rev. Mater. Res. Vol. 46, 2016, pp. 151 – 186.
[44] [iso52921] ISO/ASTM 52921-13 Standard Terminology for Additive Manufacturing - Coordinate Systems and Test Methodologies, International Organisation for Standardization, 2019.
[45] [Cheng2017] Cheng, H., Lu, C., Liu, J., et al., "Synchrotron radiation X-ray powder diffraction techniques applied in hydrogen storage materials - A review," Progress in Natural Science: Materials International, Vol. 27, 2017, pp. 66 – 73.
[46] [Mani 2017-2] Mani, M., Lane, B., Donmez, A., Feng, S., and Moylan, S., "A Review on Measurement Science Needs for Real-time Control of Additive Manufacturing Metal Powder Bed Fusion Processes," International Journal of Production Research, Volume 55, Issue 5, 2017, pp. 1400-1418.